Ultrasensitive Self-Powered Solar-Blind Deep-Ultraviolet Photodetector Based on All-Solid-State Polyaniline/MgZnO Bilayer

*Hongyu Chen, Pingping Yu, Zhenzhong Zhang, Feng Teng, Lingxia Zheng, Kai Hu, and Xiaosheng Fang**

Because of the stratospheric ozone layer surrounding the earth absorbs high-energy ultraviolet radiation, photodetectors operating in deep-ultraviolet (DUV) solar-blind region (220–280 nm) avoiding interference from solar radiation have received significant attention.[1–3] Up to now, they have led to significant progresses in the development of applications in flame sensing, chemical/biological agents detection, missile plume sensing, air/water purification, ozone layer monitoring, secure intersatellite communications, as well as underwater/submarine communication systems, and so forth.[4–10] Generally, to achieve a desirable photodetection result, traditional DUV photodetectors are in need of external power supply, which not only greatly increase the system size and energy consumption but also greatly limit their long-term working in some unmanned hazardous atmosphere or harsh environment. However, self-powered DUV photodetectors capable of operating without any power supply are still lacking up to now.

Nowadays, much efforts have been carried out for constructing UV self-powered photodetectors. Briefly, they mainly fall into two broad categories in the view of energy conversion.[2] One approach is fabricating a photodetector including an integrated power pack, which is mainly consisting of energy conversion or storage devices such as nanogenerators or fuel cells. These kinds of devices achieve the UV detection by transforming optical radiation into electrical energy along with mechanical energy or chemical energy.[11–14] However, these devices with excellent self-powered properties are almost operating in near UV region. There are lots of difficulties for expanding their work wavelength into DUV solar-blind region. For instance, nanogenerators need the materials with an excellent photoelectric property and a high piezoelectric coefficient at the same time, which limits the selecting scope of semiconductors. Meanwhile, photoelectrochemical UV photodetectors usually operate in the liquid environment, which will greatly limit the scope of their applications. In addition, self-powered photodetection achieved by traditional photovoltaic devices in terms of p–n junctions, heterojunctions, and Schottky junctions is another alternative stratagem. These kinds of devices could separate photogenerated electron–hole pairs by built-in electric field, which could transform UV radiation into electrical energy directly.[15–19] However, they possess many urgent issues to be resolved, such as realizing high quality and stable p–n homojunctions (heterojunctions) as well as modifing the poor electrode contacts in vertical Schottky photodiodes. Therefore, all-solid-state DUV self-powered photodetectors fabricated by a simple method are greatly needed.

Compared with AlGaN, diamond, TiO_2, and Ga_2O_3, etc. wide band gap semiconductor materials as well as hybrid materials like $CH_3NH_3PbCl_3$,[3,20] MgZnO alloys (**Figure 1**a,b) offer a great many advantages in fabricating DUV solar-blind photodetectors such as environmental friendly, biocompatible, large tunable band gap (≈3.3–7.8 eV) by changing $Mg_xZn_{1-x}O$ ($0 < x < 1$) with different Mg contents, and low growth temperature (100–750 °C). It is worth pointing out that albeit many issues to be solved (e.g., the lack of high quality and stable p-type MgZnO as well as high-quality single Schottky junction), MgZnO-based photodetectors covering the whole solar-blind spectrum range were realized in 2008.[9] However, these metal–semiconductor–metal structure photodetectors are constructed by two symmetric Schottky configuration, an external power source is still required to generate photocurrent. Therefore, constructing a suitable heterojunction maybe a more appropriate choice to realize MgZnO based self-powered solar-blind photodetector, more specifically, incorporating MgZnO with an excellent p-type material especially transparent in solar-blind region may be a promising pathway to solve this issue. As is well known, polyaniline (PANI) is an excellent p-type conducting polymer (Figure 1c), its hole mobilities could be tailored from 10^{-6} to 3.36 $cm^2 V^{-1} s^{-1}$ by different dopant type and oxidation state,[21–25] and then its electrical conductivities could be tailored over many orders of magnitudes as well. Hence, it has been widely used

Dr. H. Y. Chen, Dr. P. P. Yu, Dr. F. Teng, Dr. L. X. Zheng, K. Hu, Prof. X. S. Fang
Department of Materials Science
Fudan University
Shanghai 200433, P. R. China
E-mail: xshfang@fudan.edu.cn
Prof. Z. Z. Zhang
State Key Laboratory of Luminescence and Applications
Changchun Institute of Optics
Fine Mechanics and Physics
Chinese Academy of Sciences
Changchun 130033, P. R. China

DOI: 10.1002/smll.201601913

www.MaterialsViews.com

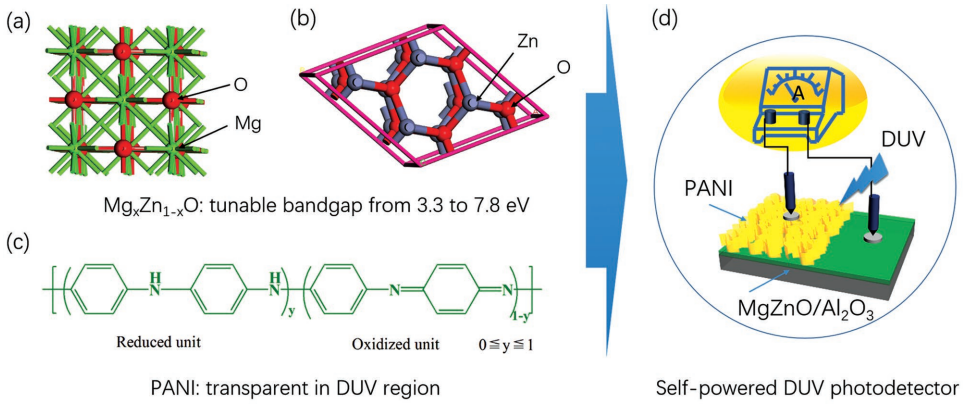

Figure 1. Schematic illustration of constructing self-powered solar-blind DUV photodetector by integrated MgZnO alloy films and PANI nanoclusters. a) MgO cubic crystal structure. b) ZnO wurtzite crystal. The band gap of MgZnO alloy could be tuned by changing $Mg_xZn_{1-x}O$ with different Mg contents. c) Molecular geometry of doped PANI. d) Configuration of PANI/MgZnO DUV photodetector operates without external bias voltage.

in supercapacitor and lithium ion battery as electrode material up to now.[26–28] Moreover, doped PANI nanofilms allow most of incident DUV light to pass through themselves in the solar-blind region (details will be demonstrated in the following text), which is beneficial for fabricating doped PANI nanofilms on a high crystal quality MgZnO alloy film by a simple transferring method. Therefore, to take full advantage of the optical and electrical characteristics of MgZnO alloy and doped PANI, we proposed a novel self-powered solar-blind photodetector based on an organic–inorganic hybrid p–n junction (Figure 1d). By fabricating the vertically aligned dense doped PANI nanofilms on the tailored MgZnO film as a hole transporting layer, the device achieves a high self-powered on/off ratio of $\approx 10^4$ under a relatively weak light intensity of illumination (250 nm, 130 μW cm^{-2}). This result obtained under zero bias voltage is comparable with the best results from other UV detection materials even at a bias voltage.[4,7,10,29,30] Its maximum responsivity is 160 μA W^{-1} at the wavelength of 250 nm with a cutoff at 271 nm at 0 V bias, and this value is comparable to that of recent reported Ga_2O_3 Schottky diode (0.01 mA W^{-1}).[31] Furthermore, owning to the unique electrical and optical properties of PANI nanofilms, the UV/visible rejection ratio of this hybrid device is up to $\approx 10^4$ which is comparable to that of previous excellent solar-blind photodetectors even at a bias voltage.[32] In addition, the bilayer photodetector operating at low bias still possesses a low dark current of 0.44 pA and a high detectivity of 1.5×10^{11} cm $Hz^{1/2}$ W^{-1}, which exhibits great potential application in detecting weak signal in the solar-blind region. Our findings indicate that constructing this simple organic–inorganic hybrid p–n junction would open up additional opportunities for fabricating high-sensitivity and energy-efficient DUV photodetectors.

In order to fabricate an excellent self-powered DUV photodetector, MgZnO epilayers with high crystal quality were employed as the active layers of the device. Meanwhile, conductive PANI nanofilms were fabricated as a hole transporting layer. Top view scanning electron microscope (SEM) images of MgZnO films at different magnifications are shown in **Figure 2**a,b, revealing a uniform and smooth film surface. Very small amounts of hexagonal grains are found to be sporadically scattered among the triangular grains (Figure 2b). This is because that the composition of the $Mg_xZn_{1-x}O$ alloy films determined by energy-dispersive x-ray spectroscopy (EDX) is $Mg_{0.44}Zn_{0.56}O$. It is just in the vicinity of critical section of structural phase transition between wurtzite and cubic.[33] It is worth pointing out that high-performance solar-blind ultraviolet photodetectors based on mixed-phase ZnMgO were reported, which performance is even better than that of single-crystalline cubic MgZnO-based photodetector.[32,34,35] These results demonstrated that the interface defect and deep defects may also partly contribute to the long lifetime of holes and the photoconductive gain. Therefore, $Mg_{0.44}Zn_{0.56}O$ films with a slight mixed-phase in this work may be beneficial for fabricating a high performance solar-blind photodetector. Topography of above mentioned MgZnO film is characterized by a typical tapping-mode atomic force microscopy (AFM), which is to further investigate the surface properties of the MgZnO films (Figure 2c), and the corresponding cross-sectional profile of the sample is shown in Figure 2d. AFM results demonstrate that the root-mean-square roughness of the MgZnO epilayer over a 1 μm × 1 μm area is ≈12.1 nm. It means that the film is fabricated with a relatively smooth surface. Figure 2e shows a typical transmission electron microscopy (TEM) image of pristine PANI nanostructures collected in the ethanol aqueous solution. These PANI samples form a networking morphology by several nanowires. Fourier transform infrared spectroscopy (FTIR) spectrum is performed to further confirm the PANI molecular structure and the results are shown in Figure 2f, and the peaks are marked out as well. The bands at 1562 and 1483 cm^{-1} are assigned to C=C stretching vibrations of quinoid and benzenoid rings, respectively. And the bands at 800 and 1107 cm^{-1} are assigned to C–H stretching vibrations of quinoid and benzenoid rings, respectively. In addition, the bands of aromatic C–N stretching vibrations at 1295 cm^{-1} of benzenoid rings and C=N stretching vibrations quinoid rings at 1237 cm^{-1} can also be clearly recognized, respectively, in consistent with the PANI molecules illustrated in Figure 1c.[36,37] The FTIR results indicate that the PANI nanoclusters are in their hole conduction state. And then, PANI/MgZnO hybrid p–n junction was fabricated, it consists of ≈120 nm PANI nanofilms on

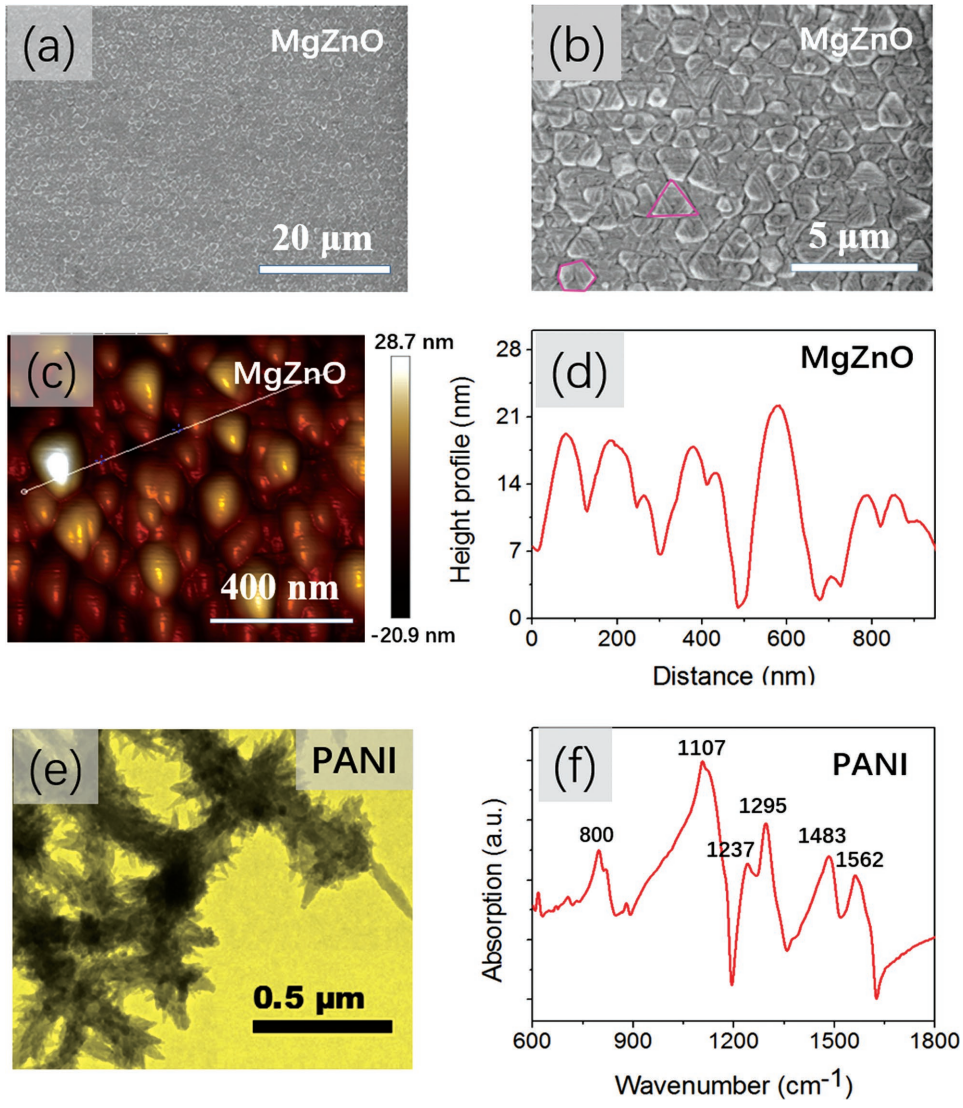

Figure 2. a,b) Typical SEM images of the MgZnO films at different magnifications. c,d) AFM image and section analysis of the MgZnO films. e) TEM image of the pristine PANI nanostructures collected in the ethanol aqueous solution. f) FTIR spectrum of PANI nanostructures, and the peaks are marked out.

the 400 nm MgZnO films. **Figure 3**a,b shows the typical SEM image of PANI/MgZnO junction boundary and the high-resolution image of PANI samples formed on the MgZnO films. It can be found that the collective PANI nanofilms are composed of vertically aligned nanoblossoms on a smooth flat surface of MgZnO. AFM image and associated section analysis (Figure 3c,d) demonstrate that these petals are well spaced from each other, and the separation between two successive petals is in the range of 200–1000 nm, the height variation of the film is ≈120 nm excepting marginal effect. This indicates that the nanofilm is highly open-structured, this would make the p–n junction in favor of yielding higher light sensitivity and longer photocarrier lifetime due to surface states. The structural characterizations of the pristine MgZnO and PANI/MgZnO p–n junction were assessed by x-ray diffraction (XRD) patterns. As shown in Figure 3e, besides the diffraction peaks from the substrate (c-Al_2O_3: 41.5°), indium electrode (33.1°, 36.1°, and 39.3°), just a strong peak at about 36.6° and a weak peak around 34.6° can be observed in both samples, corresponding to the diffraction of cubic MgZnO (111) and wurtzite MgZnO (0002), respectively.[38] The XRD result indicates the MgZnO layer has crystallized in an alight mixed-phase structure with (111) preferred orientation, which is in well agreement with the SEM image in Figure 2b. And the additional weak peak of PANI/MgZnO sample at about 24.2° is related to the periodicity parallel to the polymer chain of PANI.[36] Raman spectroscopy was performed to further examine the existence of PANI in the samples, which exhibits the same pattern in the 800–1800 cm^{-1} region. As shown in Figure 3f, the characteristic peaks located at 1170, 1230, 1337, 1480, and 1596 cm^{-1} for p–n junction samples can be attributed to C–H bonding of the quinoid ring, C–N vibration of the benzene diamine units, C=N vibration of the quinoid nanoprotonated diamine units, C=C vibration of the quinoid rings, and C–C stretching of the benzenoid ring, respectively.[36,39,40] It is in excellent agreement with that of pure PANI sample (see Figure S1, Supporting Information). This reveals the successful incorporation of PANI species with the MgZnO films.

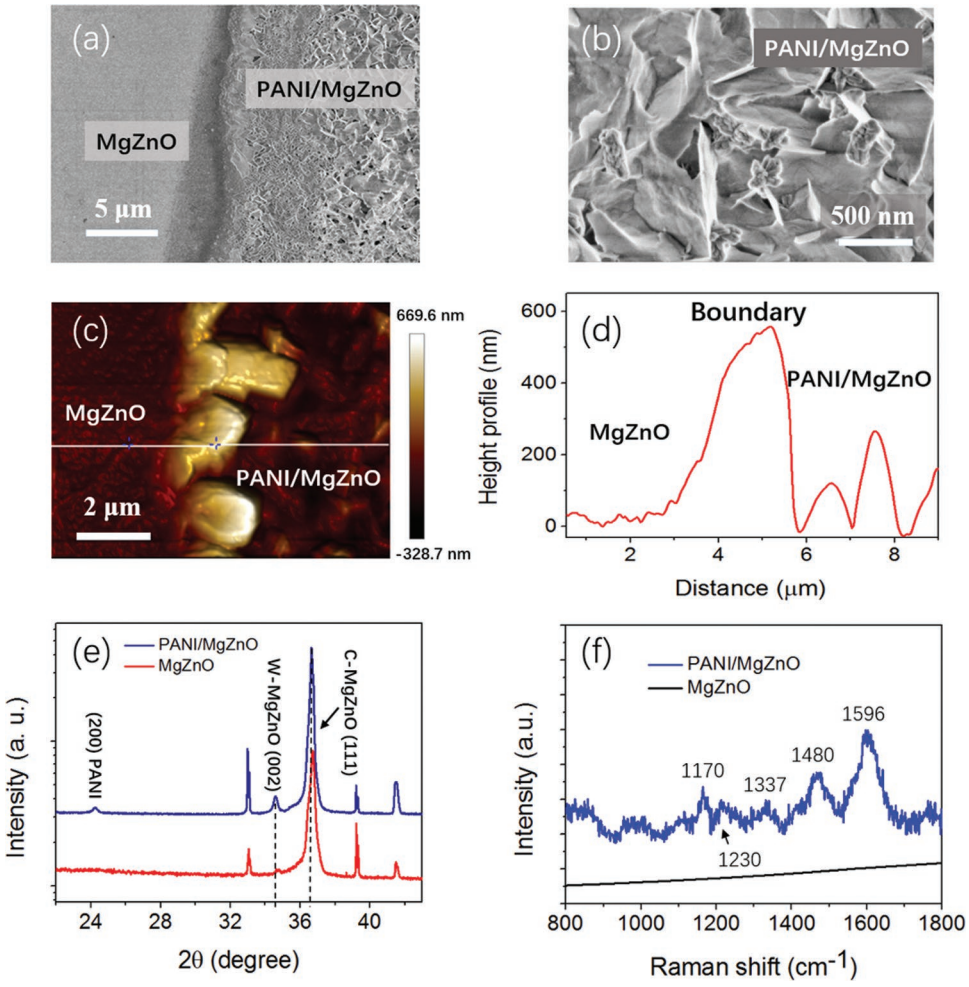

Figure 3. a) SEM image of the MgZnO/PANI boundary. b) Top view SEM image of PANI on the MgZnO films. c) AFM image of the PANI/MgZnO films. d) Section analyses of the sample in (c). e) XRD patterns of the pristine MgZnO sample and PANI/MgZnO bilayer. f) Raman spectra of MgZnO and PANI/MgZnO bilayer.

In order to explore the usefulness of the PANI/MgZnO bilayer in high-performance self-powered DUV optoelectronic devices, a typical *I–V* curve of the PANI/MgZnO hybrid p–n junction photodetector is shown in **Figure 4**a (inset of Figure 4a is the side view of the device). The current shows a significant rectification characteristic with a turn-on voltage of about 2.5 V, indicating a typical photodiode behavior. Figure 4b gives the *I–V* plots from the In–p–PANI and In–n–MgZnO contacts (*I–V* curves in logarithmic coordinates are in Figure S2, Supporting Information), indicating both p and n electrodes are excellent Ohmic contacts. These results demonstrate that the rectifying behavior comes from the p–n junction instead of the metal–semiconductor contacts. Moreover, albeit doped PANI is an excellent conducting polymer, the hybrid PANI/MgZnO p–n junction device still exhibits a very low dark current of 0.44 pA even under a bias of –1 V, which is comparable to that of pristine MgZnO device (0.15 pA) and previous best results of solar-blind photodetectors.[4–10,29,32] To examine the self-powered character of this diode in DUV region, Figure 4c shows the on/off cycles of the reference MgZnO device at a bias of –1 V (top) and PANI/MgZnO hybrid p–n junction device at 0 V (bottom) upon 250 nm light illumination. It can be observed that the photocurrent (≈15.4 pA) of diode without any power supply is comparable to that of pristine MgZnO device (≈14.2 pA) at –1 V. In addition, the current changes four orders of magnitude immediately with well-reproducible and highly stable (an amplificatory dark current of PANI/MgZnO hybrid p–n junction device is shown in Figure 4d) when the transition between DUV light on and off takes place. This result obtained under zero bias voltage is comparable with that of previous excellent solar-blind photodetectors even at a bias voltage.[10–30] To further explore the signal-to-noise ratio of this self-powered photodetector, linear dynamic range (LDR, typically quoted in dB) is an important figure-of-merits. A high LDR indicates a device having a relatively large ratio of photocurrent to dark current. Generally, LDR can be obtained from the equation[29]

$$\mathrm{LDR} = 20\log(I_\mathrm{p}/I_\mathrm{d}) \quad (1)$$

where I_p is the photocurrent obtained at the wavelength of 250 nm with the intensity of 0.13 mW cm^{-2}, I_d is the dark current. The calculated LDR (80 dB) is larger than that of InGaAs based photodetectors (66 dB).[41] To further confirm its rectification characteristics, we also observed that the

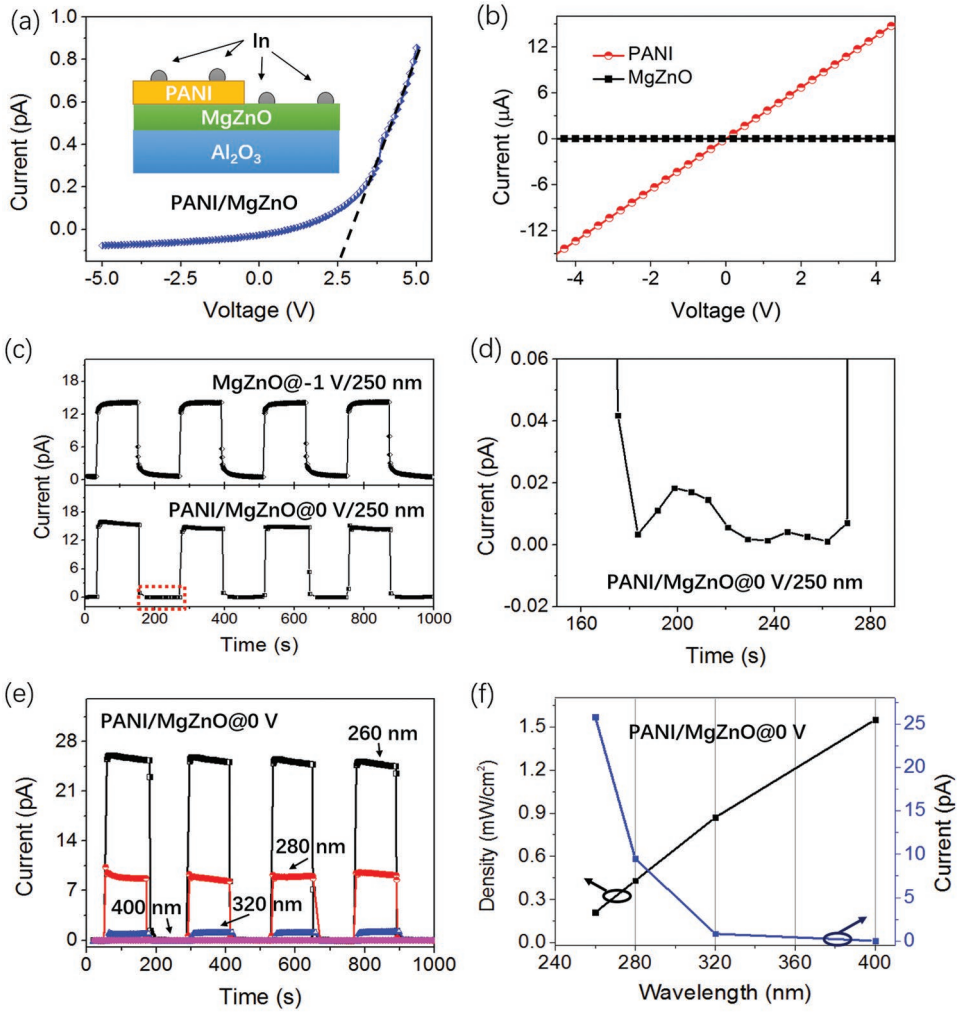

Figure 4. a) Typical *I–V* curve for the PANI/MgZnO device under dark condition. b) *I–V* curves for the MgZnO and PANI device under dark condition. c) Reproducible on/off switching of MgZnO photodetector upon 250 nm (0.13 mW cm^{-2}) light at a bias of –1 V (top), reproducible on/off switching of PANI/MgZnO photodetector upon 250 nm (0.13 mW cm^{-2}) light at a bias of 0 V(bottom). d) Amplification of the dark current for photodetector in the red dashed box in (c). e) The reproducible on/off switching upon 260 nm (0.21 mW cm^{-2}), 280 nm (0.43 mW cm^{-2}), 320 nm (0.87 mW cm^{-2}), and 400 nm (1.55 mW cm^{-2}) light illumination. f) Photocurrent and optical power density as a function of the excitation wavelength.

binary-photocurrent changes from positive to negative with the same magnitude upon illumination when grounding electrode is exchanging (not show here). The 10%–90% rise time and decay time of pristine MgZnO were measured (–1 V) to be ≈4.8 and ≈5.1 s, respectively, while due to the build-in internal electric field of p–n junction, both the rise and decay times of PANI/MgZnO diode (0 V) are less than 0.3 s (limitation of the measurement system). Therefore, compared with the pristine MgZnO device, the PANI/MgZnO p–n photodiodes in this work have the advantage of low applied bias and fast response times, which provides an opportunity to use the device as an on–off binary-response for DUV detection. To further confirm the excellent on/off switching properties in the DUV region, Figure 4e shows the on/off switching currents upon with solar-blind lights (260 nm: 0.21 mW cm^{-2}, 280 nm: 0.43 mW cm^{-2}), a UVB light (320 nm: 0.87 mW cm^{-2}), and a visible light (400 nm: 1.55 mW cm^{-2}) illumination at 0 V, respectively. Although the optical power density (Figure 4f) is increased, the photocurrents are decreased from DUV to near UV region, even the on/off switching currents under 400 nm light illumination nearly without any photoresponse, staying at the off state, indicating this device is operated with an excellent wavelength selective property. To further explore its working wavelength range, the spectra responsivity ranging from 220 to 500 nm was obtained critically at 0 V bias as follows

$$R_\lambda = \frac{I_p}{P} \tag{2}$$

where I_p is the photocurrent, which is the difference between the light current and dark current, P is the incident irradiation power, and λ is the excitation wavelength. As shown in **Figure 5**a, the maximum responsivity of the photodetector is 160 μA W^{-1} at the wavelength of 250 nm with a cutoff wavelength at 271 nm, which is comparable to that of pristine MgZnO device works at –1 V. Moreover, this responsivity is comparable to that of recent reported Ga_2O_3 based

www.MaterialsViews.com

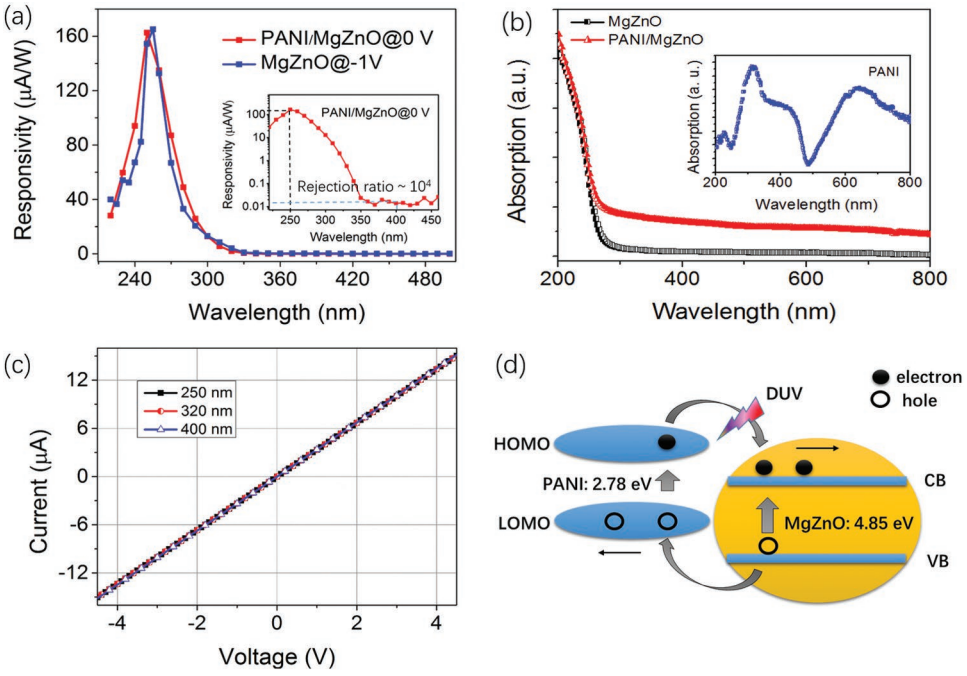

Figure 5. a) Spectral response of reference MgZnO photodetector at –1 V bias and PANI/MgZnO photodetector at 0 V bias. The inset shows the spectral response of PANI/MgZnO diode in logarithmic scale. b) Absorption spectra of MgZnO layer and PANI/MgZnO bilayer, and the inset is absorption spectrum of PANI layer. c) *I–V* curve for the PANI under different illuminations (250 nm: 0.13 mW cm^{-2}, 320 nm: 0.87 mW cm^{-2}, and 400 nm: 1.55 mW cm^{-2}). d) Band alignment of the PANI/MgZnO type-II heterojunction.

self-powered solar-blind photodetector.[31] In addition, the UV–visible rejection ratio (R_{250}/R_{400}) is around four orders of magnitude. This result obtained under zero bias voltage is comparable with the best results from any other solar-blind detection materials even at a bias voltage.[4–6,10,29,31,32] The detectivity (D^*) is one of the key figure-of-merits for a photodetector, which usually describes the smallest detectable signal. D^* is defined as

$$D^* = \frac{(A\Delta f)^{1/2} R_\lambda}{i_{td}} \tag{3}$$

and i_{td} is

$$i_{td} \approx i_{n,s} = \sqrt{2qI_d\Delta f} \tag{4}$$

where A is the active area, Δf is the bandwidth, i_{td} is the total noise current, and I_d is the dark current.[41] For solar-blind photodetectors operated by low driven voltage, background radiation has little effect on the device noise, and the thermal-related noise current at 300 K is calculated ≈10^{-15} A.[42,43] In this case, the shot noise is the major contributor to the total noise.[29,41,44,45] Consequently, detectivity of a DUV photodetector can be written as

$$D^* = \frac{R_\lambda}{(2qI_d/A)^{1/2}} \tag{5}$$

and detectivity of the heterostructured device is as high as 1.5×10^{11} cm Hz$^{1/2}$ W^{-1} even under a small bias (–1 V) at the wavelength of 250 nm with a low intensity of 0.13 mW cm^{-1}. These results show that this organic (PANI) and inorganic (MgZnO) hybrid p–n junction structure device has great potential application in solar-blind DUV detection with low energy consumption. Especially, it is worth pointing out that albeit PANI is on the surface of MgZnO, the cutoff edge of hybrid p–n junction is the same as that of pristine MgZnO single layer. In order to get more insight into the underlying physics of this special phenomenon and shed light on the origin of photocurrent at 0 V bias voltage, UV–visible absorption spectra of PANI, MgZnO, and PANI/MgZnO bilayer are examined. As shown in Figure 5b, although doped PANI has a weak absorption peak at ≈225 nm and a relatively stronger absorption peak at ≈315 nm in the UV region due to the π–π^* transition of the benzenoid rings,[46–48] and in spite of the absorption of the PANI/MgZnO bilayer is larger than that of pristine MgZnO when the wavelength is longer than 280 nm, the absorption edges of both samples are around 256 nm, indicating PANI in superstratum of PANI/MgZnO bilayer has little or none impact on absorption light of MgZnO films in solar-blind region. To further explore the photoelectric property of PANI sample, *I–V* characteristics of PANI nanofilms are carried out under illuminated with a solar-blind light (250 nm: 0.13 mW cm^{-2}), a UVB light (320 nm: 0.87 mW cm^{-2}), and a visible light (400 nm: 1.55 mW cm^{-2}). As shown in Figure 5c, the light current of PANI is the same as its dark current at any wavelength light (Figures 4b and 5c). Hence, in conjunction with the band alignment of the PANI/MgZnO type-II heterojunction in Figure 5d, a possible operating mechanism of the self-powered photodetector is proposed. Under DUV irradiation, the photocurrent is mainly extracted from the photocarriers in the active layer of MgZnO. Due to PANI nanoclusters can

function as a "transparent" conducting path in the solar-blind region, DUV radiation with the wavelength smaller than 280 nm may almost pass through the PANI layer to create electron–hole pairs in the MgZnO, and photocarriers are quickly separated by the built-in electric field of PANI/MgZnO junction to yield a photocurrent. In addition, a portion of valence electrons in the valence band (VB) of MgZnO would be excited to the lower unoccupied molecular orbital (LOMO) of PANI, and then excited to the highest occupied molecular orbital (HOMO) of PANI, subsequently transited to the conduction band (CB) of MgZnO. This electron transition process can restrain the electron–hole recombination within MgZnO, which largely enhances photocurrent. However, if the incident light is longer than 280 nm, the optical radiation energy is too small to create electron–hole pairs in the MgZnO, and the PANI has no photoresponse at any wavelength in this work, that is why the cutoff edge of PANI/MgZnO hybrid p–n photodetector is the same as the pristine MgZnO device (Figure 5a).

In summary, a high-sensitivity self-powered solar-blind DUV photodetector based on hybrid organic PANI and inorganic MgZnO bilayer with a sharp cutoff at 271 nm is realized in this work. Due to the superior properties of the hybrid p–n junction, these photodetectors with a simple bilayer structure exhibit high on/off ratios (10^4) at a relatively weak light intensity of 130 mW cm^{-2}. This result obtained under zero bias voltage is comparable to that of previous best solar-blind photodetectors even at a bias voltage. The responsivity of the photodetector is 160 μA W^{-1} at the wavelength of 250 nm, which is comparable to that of recent reported Ga_2O_3 based self-powered solar-blind photodetector. Its UV/visible (250/400 nm) rejection ratio is achieved up to ≈10^4, which is almost three orders of magnitude larger than that of Ga_2O_3 Schottky diode. Moreover, the low dark current (0.44 pA) and high detectivity (1.5×10^{11} cm $Hz^{1/2}$ W^{-1}) at low bias voltage (–1 V) is comparable to that of previous excellent solar-blind photodetectors. The results reported in this paper provide a facile route to construct all-solid-state organic/inorganic p–n junction DUV photodetectors with high-sensitivity and low energy consumption. Thus, this work may lay a solid ground for the future applications of this kind of photodetectors.

Experimental Section

Material Synthesis and Device Fabrication: In this work, the MgZnO epilayer was fabricated as our previous work.[49,50] Briefly, it was deposited directly on a c-plane (0001) sapphire substrate by metal organic chemical vapor deposition at 450 °C, with the pressure of 2×10^4 Pa. Highly pure oxygen (99.999%), diethylzinc (DEZn), and dimethyl dicyclopentadienyl magnesium ($(MeCp)_2Mg$) were employed as the precursors and highly pure nitrogen (99.999%) was used as the carrier gas. Meanwhile, aniline (AN, 45.65 μL) was added to 40 mL of 1 m H_2SO_4 aqueous solution and then stirred for 20 min to ensure complete dispersion at 0 °C. Another 40 mL of 1 m H_2SO_4 cold aqueous solution containing ammonium peroxydisulfate (APS, 114.12 mg) was rapidly added and stirred for 1 min. The molar ratio of AN to APS was 1:1. The polymerization carried out at 0 °C for 24 h, and the obtained PANI nanocluster was washed with deionized water for several times, and then transferred to the surface of MgZnO film. After drying at 80 °C for 12 h, the indium electrodes were fabricated on MgZnO and PANI layers, respectively.

Analysis Instruments: Sample morphologies were characterized using field-emission scanning electron microscopy (Hitachi, S4800), AFM (Bruker, MultiMode-8), and a TEM (Tecnai G^2 S-TWIN). EDX was used to determine the composition of the MgZnO films, and their crystal structure and chemical bonding characteristics were studied using a Bruker D8-A25 diffractometer using Cu Kα radiation (λ = 1.5405 Å), Raman spectroscopy (Spex 403 Raman microscope with 532 nm argon ion laser), and FTIR spectroscopy (Nicolet Nexus 470). The optical properties were investigated by optical diffuse absorption spectra using a UV–vis spectrophotometer (Hitachi, U-3900H) with an integrating sphere attachment. The photoelectric performance was analyzed with a Xe lamp, monochromator, and a program-controlled semiconductor characterization system (Keithley 4200 and 4200 remote preamps), respectively.

Supporting Information

Supporting Information is available from the Wiley Online Library or from the author.

Acknowledgements

The authors thank Dr. Dandan Wang, Yanmei Li, and Dr. Bin Zhao for their technical assistance and kind help. This work is supported by the National Natural Science Foundation of China (Grant Nos. 61376054, 51471051, and 61505033), National Postdoctoral Science Foundation of China (Grant Nos. 2015M571487, 2015M580294, and 2016T90336), Science and Technology Commission of Shanghai Municipality (15520720700), Shanghai Shu Guang Project (12SG01), and the Programs for Professor of Special Appointment (Eastern Scholar) at Shanghai Institutions of Higher Learning.

[1] H. Y. Chen, H. Liu, Z. M. Zhang, K. Hu, X. S. Fang, *Adv. Mater.* **2016**, *28*, 403.
[2] H. Y. Chen, K. W. Liu, L. F. Hu, A. A. Al-Ghamdi, X. S. Fang, *Mater. Today* **2015**, *18*, 493.
[3] E. Monroy, F. Omnès, F. Calle, *Semicond. Sci. Technol.* **2003**, *18*, R33.
[4] Y. Guo, C. Liu, H. Tanaka, E. Nakamura, *J. Phys. Chem. Lett.* **2015**, *6*, 535.
[5] X. Du, Z. Mei, Z. Liu, Y. Guo, T. Zhang, Y. Hou, Z. Zhang, Q. Xue, A. Y. Kuznetsov, *Adv. Mater.* **2009**, *21*, 4625.
[6] G. Parish, S. Keller, P. Kozodoy, J. P. Ibbetson, H. Marchand, P. T. Fini, S. B. Fleischer, S. P. DenBaars, U. K. Mishra, E. J. Tarsa, *Appl. Phys. Lett.* **1999**, *75*, 247.
[7] X. S. Fang, L. F. Hu, K. F. Huo, B. Gao, L. J. Zhao, M. Y. Liao, P. K. Chu, Y. Bando, D. Golberg, *Adv. Funct. Mater.* **2011**, *21*, 3907.

[8] E. Ozbay, N. Biyikli, I. Kimukin, T. Kartaloglu, T. Tut, O. Aytur, *IEEE J. Sel. Top. Quantum Electron.* **2004**, *10*, 742.
[9] Z. G. Ju, C. X. Shan, D. Y. Jiang, J. Y. Zhang, B. Yao, D. X. Zhao, D. Z. Shen, X. W. Fan, *Appl. Phys. Lett.* **2008**, *93*, 173505.
[10] L. Li, P. S. Lee, C. Yan, T. Y. Zhai, X. S. Fang, M. Y. Liao, Y. Koide, Y. Bando, D. Golberg, *Adv. Mater.* **2010**, *22*, 5145.
[11] J. Zhou, L. Chen, Y. Wang, Y. He, X. Pan, E. Xie, *Nanoscale* **2016**, *8*, 50.
[12] Q. Yang, Y. Liu, Z. Li, Z. Yang, X. Wang, Z. L. Wang, *Angew. Chem. Int. Ed.* **2012**, *51*, 6443.
[13] L. Peng, L. F. Hu, X. S. Fang, *Adv. Mater.* **2013**, *25*, 5321.
[14] X. Li, C. Gao, H. Duan, B. Lu, X. Pan, E. Xie, *Nano Energy* **2012**, *1*, 640.
[15] H. Y. Chen, K. Liu, X. Chen, Z. Zhang, M. Fan, M. Jiang, X. Xie, H. Zhao, D. Shen, *J. Mater. Chem. C* **2014**, *2*, 9689.
[16] Y. Chen, C. Wang, G. Chen, Y. Li, C. Liu, *Nano Energy* **2015**, *11*, 533.
[17] Y. Bie, Z. Liao, H. Zhang, G. Li, Y. Ye, Y. Zhou, J. Xu, Z. Qin, L. Dai, D. Yu, *Adv. Mater.* **2011**, *23*, 649.
[18] D. Xiang, C. Han, Z. Hu, B. Lei, Y. Liu, L. Wang, W. P. Hu, W. Chen, *Small* **2015**, *11*, 4829.
[19] X. Chen, K. Ruan, G. Wu, D. Bao, *Appl. Phys. Lett.* **2008**, *93*, 112112.
[20] G. Maculan, A. D. Sheikh, A. L. Abdelhady, M. I. Saidaminov, M. A. Haque, B. Murali, E. Alarousu, O. F. Mohammed, T. Wu, O. M. Bakr, *J. Phys. Chem. Lett.* **2015**, *6*, 3781.
[21] Y. Li, Y. Lin, C. Wei, Y. Wang, *Solid State Electron.* **2013**, *79*, 56.
[22] S. Bhadra, S. Chattopadhyay, N. K. Singha, D. Khastgir, *J. Appl. Polym. Sci.* **2008**, *108*, 57.
[23] S. E. Bourdo, V. Saini, J. Piron, I. Al-Brahim, C. Boyer, J. Rioux, V. Bairi, A. S. Biris, T. Viswanathan, *ACS Appl. Mater. Interfaces* **2012**, *4*, 363.
[24] H. Wang, S. Yi, X. Pu, C. Yu, *ACS Appl. Mater. Interfaces* **2015**, *7*, 9589.
[25] K. P. Nazeer, S. A. Jacob, M. Thamilselvan, D. Mangalaraj, S. K. Narayandass, J. Yi, *Polym. Int.* **2004**, *53*, 898.
[26] J. M. Jeong, B. G. Choi, S. C. Lee, K. G. Lee, S. J. Chang, Y. K. Han, Y. B. Lee, H. U. Lee, S. Kwon, G. Lee, *Adv. Mater.* **2013**, *25*, 6250.
[27] X. H. Huang, J. P. Tu, X. H. Xia, X. L. Wang, J. Y. Xiang, *Electrochem. Commun.* **2008**, *10*, 1288.
[28] Q. Wu, Y. Xu, Z. Yao, A. Liu, G. Shi, *ACS Nano* **2010**, *4*, 1963.
[29] B. Zhao, F. Wang, H. Chen, Y. Wang, M. Jiang, X. Fang, D. Zhao, *Nano Lett.* **2015**, *15*, 3988.
[30] J. Xing, E. Guo, K. Jin, H. Lu, J. Wen, G. Yang, *Opt. Lett.* **2009**, *34*, 1675.
[31] X. Chen, K. Liu, Z. Zhang, C. Wang, B. Li, H. Zhao, D. Zhao, D. Shen, *ACS Appl. Mater. Interfaces* **2016**, *8*, 4185.
[32] L. K. Wang, Z. G. Ju, J. Y. Zhang, J. Zheng, D. Z. Shen, B. Yao, D. X. Zhao, Z. Z. Zhang, B. H. Li, C. X. Shan, *Appl. Phys. Lett.* **2009**, *95*, 131113.
[33] S. Choopun, R. D. Vispute, W. Yang, R. P. Sharma, T. Venkatesan, H. Shen, *Appl. Phys. Lett.* **2002**, *80*, 1529.
[34] M. M. Fan, K. W. Liu, Z. Z. Zhang, B. H. Li, X. Chen, D. X. Zhao, C. X. Shan, D. Z. Shen, *Appl. Phys. Lett.* **2014**, *105*, 11117.
[35] M. Fan, K. Liu, X. Chen, X. Wang, Z. Zhang, B. Li, D. Shen, *ACS Appl. Mater. Interfaces* **2015**, *7*, 20600.
[36] P. Yu, Y. Li, X. Zhao, L. Wu, Q. Zhang, *Synthetic Met.* **2013**, *185–186*, 89.
[37] N. S. Sariciftci, M. Bartonek, H. Kuzmany, H. Neugebauer, A. Neckel, *Synthetic Met.* **1989**, *29*, 193.
[38] X. H. Xie, Z. Z. Zhang, C. X. Shan, H. Y. Chen, D. Z. Shen, *Appl. Phys. Lett.* **2012**, *101*, 81104.
[39] H. Fan, H. Wang, N. Zhao, X. Zhang, J. Xu, *J. Mater. Chem.* **2012**, *22*, 2774.
[40] M. Dhingra, L. Kumar, S. Shrivastava, P. S. Kumar, S. Annapoorni, *Bull. Mater. Sci.* **2013**, *36*, 647.
[41] S. Liu, Z. Wei, Y. Cao, L. Gan, Z. Wang, W. Xu, X. Guo, D. Zhu, *Chem. Sci.* **2011**, *2*, 796.
[42] Z. Ning, X. Gong, R. Comin, G. Walters, F. Fan, O. Voznyy, E. Yassitepe, A. Buin, S. Hoogland, E. H. Sargent, *Nature* **2015**, *523*, 324.
[43] Y. Fang, J. Huang, *Adv. Mater.* **2015**, *27*, 2804.
[44] L. Shen, Y. Fang, H. Wei, Y. Yuan, J. Huang, *Adv. Mater.* **2016**, *28*, 2043.
[45] C. Ma, Y. Shi, W. Hu, M. Chiu, Z. Liu, A. Bera, F. Li, H. Wang, L. Li, T. Wu, *Adv. Mater.* **2016**, *28*, 3683.
[46] S. Weng, Z. Lin, L. Chen, J. Zhou, *Electrochim. Acta* **2010**, *55*, 2727.
[47] D. Bang, Y. W. Chang, J. Park, J. Lee, K. Yoo, Y. Huh, S. Haam, *Thin Solid Films* **2012**, *520*, 6818.
[48] Q. Tang, J. Wu, X. Sun, Q. Li, J. Lin, *Langmuir* **2009**, *25*, 5253.
[49] H. Y. Chen, K. Liu, M. Jiang, Z. Zhang, X. Xie, D. Wang, L. Liu, B. Li, D. Zhao, C. Shan, D. Shen, *Appl. Phys. Lett.* **2014**, *104*, 91119.
[50] H. Y. Chen, K. Liu, M. Jiang, Z. Zhang, L. Liu, B. Li, X. Xie, F. Wang, D. Zhao, C. Shan, *J. Phys. Chem. C* **2013**, *118*, 679.

Received: June 7, 2016
Revised: July 10, 2016
Published online: September 5, 2016